

# Compositional Zero-shot Learning via Progressive Language-based Observations

Lin Li<sup>1,2</sup>, Guikun Chen<sup>1</sup>, Jun Xiao<sup>1</sup>, Long Chen<sup>2\*</sup>

<sup>1</sup>Zhejiang University <sup>2</sup>The Hong Kong University of Science and Technology

{mukti, guikun.chen, junx}@zju.edu.cn, longchen@ust.hk

## Abstract

Compositional zero-shot learning aims to recognize unseen state-object compositions by leveraging known primitives (state and object) during training. However, effectively modeling interactions between primitives and generalizing knowledge to novel compositions remains a perennial challenge. There are two key factors: object-conditioned and state-conditioned variance, i.e., the appearance of states (or objects) can vary significantly when combined with different objects (or states). For instance, the state “old” can signify a vintage design for a “car” or an advanced age for a “cat”. In this paper, we argue that these variances can be mitigated by predicting composition categories based on pre-observed primitive. To this end, we propose Progressive Language-based Observations (PLO), which can **dynamically** determine a better observation order of primitives. These observations comprise a series of concepts or languages that allow the model to understand image content in a step-by-step manner. Specifically, PLO adopts pre-trained vision-language models (VLMs) to empower the model with observation capabilities. We further devise two variants: 1) PLO-VLM: a two-step method, where a pre-observing classifier dynamically determines the observation order of two primitives. 2) PLO-LLM: a multi-step scheme, which utilizes large language models (LLMs) to craft composition-specific prompts for step-by-step observing. Extensive ablations on three challenging datasets demonstrate the superiority of PLO compared with state-of-the-art methods, affirming its abilities in compositional recognition.

## 1. Introduction

“There’s more than one way to skin a cat.”

What enables us humans to recognize new concepts we have never encountered before? It all comes down to our capacity to generalize learned knowledge to unseen domains. For instance, when presented with concepts “green

\*Corresponding author. Work was done when Lin Li visited HKUST.

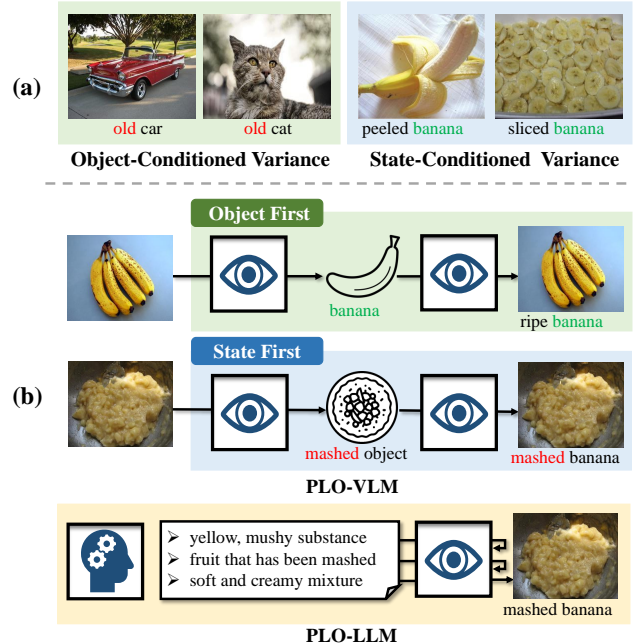


Figure 1. Illustrations of challenges in CZSL and the proposed PLO method. (a) The challenge of object/state-conditioned variation: A perceptible variance emerges in the visual appearance of state/object primitives when juxtaposed in different compositions. (b) PLO-VLM/LLM: A two/multi-step observation approach dynamically controls the observation order for effective recognition.

apple” and “yellow banana”, we can instantly recognize and imagine the concept “green banana” by combining state “green” with object “banana”. Inspired by this innate cognitive ability of humans, Compositional Zero-Shot Learning (CZSL) emerges to tackle the challenge of recognizing *unseen* state-object compositions (e.g., “green banana”) by leveraging visible primitives (i.e., state and object) in compositional concepts during training and applying the knowledge during inference [19, 25, 29].

Effectively modeling the interactions between state and object primitives, as well as extrapolating the understanding of seen compositions to unseen ones, poses major challenges in CZSL. Concretely, it revolves around two critical

factors: 1) **Object-conditioned Variance**: Wherein the visual representations of the same state category can vary considerably when different objects are involved. As depicted in Figure 1(a), considering the state “old” in the context of modifying a “car” and a “cat”, it may refer to a vintage design with classic curves and retro elements for the “car”, evoking a sense of nostalgia and history, whereas for the “cat”, it denotes the senior age of feline with features like grey fur, reflecting the passage of time and aging process. 2) **State-conditioned Variance**: It pertains to the variations in the appearance of an object when combined with different states. As shown in Figure 1(a), for composition “peeled banana”, the “banana” exhibits a smooth texture and a pale appearance, as the outer peel is removed. In contrast, for the composition “sliced banana”, the “banana” takes on a sliced appearance with visible segments.

Previous approaches in CZSL often construct separate classifiers for recognizing states and objects simultaneously, overlooking their intrinsic relationship. Recent efforts have made strides in addressing the **first factor** by adopting a two-stage method with an object-then-state order [11, 15, 36]. Prioritizing the prediction of the object primitive allows the model to capture salient visual cues (e.g., shapes), thereby enhancing the overall comprehension of compositions. Subsequently, armed with the knowledge of the object primitives, the CZSL model sequentially refines its understanding by classifying the state primitives conditioned on guided object features.

Nonetheless, we argue that *there is more than one way to skin a cat*, and the human cognition process will progressively collect different observations for specific compositions, in a *simple to complex* manner. In certain cases, such as the composition “ripe banana” in Figure 1(b), the object itself, “banana”, possesses highly salient visual cues that make it easily recognizable due to its curving shape and vibrant yellow color. Once we establish that it is a “banana”, we can then further analyze its state and recognize it as a “ripe banana” by observing additional visual cues, e.g., the presence of brown spots on the yellow skin. In contrast, for compositions like “mashed banana”, possess distinct visual features primarily related to the state “mashed” rather than the object. The mushy texture becomes the prominent aspect that captures our attention. Consequently, through further analysis of extra visual features, e.g., yellow and sticky material, we refine our recognition and discern it as a “mashed banana”.

In this paper, inspired by the human-like cognition process, we propose a novel approach, **Progressive Language-based Observations (PLO)** for CZSL. Specifically, PLO dynamically determines the order of progressive observations in the form of language, building upon the pre-trained vision-language models (VLMs), e.g., CLIP [34]. These observations comprise a series of languages that allow the

model to observe the image’s content step by step. Due to training with image-text pairs, these VLMs endow the model with *observing* capability by measuring the similarity between the two modalities within the same space. For dynamic progressive observation, we propose two variants: PLO-VLM and PLO-LLM. In **PLO-VLM**, we introduce a two-step observation strategy that adopts a pre-observing classifier based on VLM to dynamically determine the order of primitive-containing languages based on image features. Subsequently, leveraging the observed primitive knowledge (semantic features from primitive prompts), we integrate this information via a cross-modal attention module for category prediction of the remaining primitive. In **PLO-LLM**, we further extend to a multi-step observation scheme, employing large language models (LLMs), e.g., GPT [4] to design composition-specific prompts (e.g., “yellow, mushy substance” in Figure 1(b)) for each composition category, thus obtaining a composition-specific observation order. This method allows us to selectively extract features at each observation step, boosting the model’s ability to understand and recognize composition categories more effectively.

Three popular and challenging CZSL datasets MIT-States [12], UT-Zappos [29], and C-GQA [39] are used for evaluation. Extensive results show that our PLO exceeds the current state-of-the-art CZSL methods with significant gains in both closed-world and open-world settings. In summary, the main contributions of our work are three-fold:

- We propose the novel PLO for CZSL. To the best of our knowledge, it is the first work to dynamically allocate the order of observations using language, enabling effective prediction of unseen state-object compositions.
- We introduce two model variants: 1) PLO-VLM: It uses a pre-observing classifier to determine observation order based on image features. 2) PLO-LLM: It employs LLMs to design composition-specific observation prompts.
- Extensive results on multiple datasets demonstrate that PLO outperforms existing methods, showcasing its effectiveness in recognizing *unseen* state-object compositions.

## 2. Related Work

**Compositional Zero-Shot Learning (CZSL)**. CZSL is a prominent research area, and state-of-the-art methods can be broadly categorized into two directions: 1) **Composed CZSL** [2, 26, 28, 29, 33]: It focuses on directly classifying compositional state-object, which projects whole compositional visual features into a shared feature space. 2) **Decomposed CZSL** [5, 8, 13, 14, 19, 20, 40]: It disentangles visual features of simple primitives by designing two classifiers to predict state and object primitives respectively. Notably, recent breakthroughs in CZSL through CLIP-based methods (including both composed and decomposed methods) [10, 22, 23, 30]. These methods leverage frozen CLIP models to acquire textual embeddings of simple primitives,

showcasing robust compositionality for zero-shot generalization. Nevertheless, they lack systematic investigation of the intrinsic relation between states and objects, ignoring the priority of visual cues. Specifically, Troika [10] adopts a Multi-Path framework to dynamically adjust prompts based on visual features, similar to the idea of the CoCoOP [42]. However, it may not fully leverage the inherent relationship between states and objects. In contrast, our PLO innovatively determines the observation order through language, allowing for a more nuanced understanding of state-object compositions and advancing the recognition of unseen combinations. This work represents the first effort, as far as we know, that models CZSL in a simple to complex manner by progressive language-based observations.

**Large Language Models (LLMs) for CV Tasks.** LLMs have ushered in a new era for natural language understanding and reasoning. There are two main types of solutions to integrate LLMs into CV: 1) Building multi-modal LLMs. Multi-modal pre-training aligns vision and language modalities in various ways, such as fine-tuning the visual encoder [35], training additional cross-attention layers [1], or reducing the size of extra layers and pre-trained lightweight modules [17, 44]. Such *de facto* paradigms require significant computing resources and training data, hindering further applications. 2) Deriving knowledge from LLMs. They query LLMs with meticulously curated prompts to obtain valuable information such as descriptions about category [18, 27, 31] or synthesized data [9]. By such means, vision tasks can enjoy powerful implicit knowledge within LLMs. In this paper, we harness the capabilities of GPT to generate observation prompts and facilitate compositional reasoning in CZSL. By leveraging the strengths of LLMs, PLO enhances the understanding of visual compositions and provides a novel approach to address CZSL challenges.

### 3. Progressive Language-based Observations

**Formulation.** Given an image  $I$ , CZSL focuses on the recognition of images belonging to composition categories  $c \in C$ , where the category set  $C$  is defined as the Cartesian product of given state categories  $S = \{s_1, \dots, s_{|S|}\}$  and object categories  $O = \{o_1, \dots, o_{|O|}\}$ , *i.e.*,  $C = S \times O$ . During training, the models have access only to a set of seen compositions. **In closed-world testing**, the model must recognize images from both the seen compositions in  $C(s)$  and the unseen compositions in  $C(u)$ , where  $|C(s) \cup C(u)| \ll |C|$  during testing. **In open-world testing**, the model needs to recognize images from any composition within  $C$ . This scenario presents a more challenging task as the model must handle a broader range of compositions.

In this section, we first introduce how to endow models with *observing* capabilities in Sec. 3.1. Then, we describe how to determine the step-by-step observation sequence for progressive comprehension, *i.e.*, PLO-VLM and

PLO-LLM, in Sec. 3.2 and Sec. 3.3, respectively.

#### 3.1. CLIP-based Observing

To enable observing ability, our PLO builds upon a pre-trained vision-language model: CLIP [34], which consists of an image encoder  $En_v(\cdot)$  and a text encoder  $En_t(\cdot)$  capable of mapping image features and semantic features from prompts (natural languages with category information, *e.g.*, “a photo of ripe banana”) into a shared semantic space. By comparing the similarities between the two modalities in this shared space, we can discern whether language-based observations exist in a given image.

**1) Image Encoder  $En_v(\cdot)$ .** We enhance the image encoder of CLIP with some lightweight parameter efficient fine-tuning (PEFT) strategies [6, 7], allowing it to effectively handle image features in CZSL. These PEFT strategies<sup>1</sup> allow the encoder to achieve performance levels comparable to full fine-tuning by transferring knowledge from CLIP while avoiding strong training biases with several learnable parameters.

Specifically, the image encoder  $En_v(\cdot)$  splits the input image into non-overlapping patches ( $N$  in total) along with a pre-trained [CLS] token and positional embeddings, then generates a sequence of patch tokens. After that, the self-attention-based blocks, including the inserted learnable layers, are used to update the token sequence  $\mathcal{V} = \{\mathbf{v}_{[\text{CLS}]}, \mathbf{v}_1, \mathbf{v}_2, \dots, \mathbf{v}_N\}$ . By optimizing the parameters of these inserted learnable layers during training while keeping the original image encoder frozen, PLO effectively incorporates primitive-specific information to improve observation capabilities. Finally, a linear layer is utilized to project the output [CLS] token  $\hat{\mathbf{v}}_{[\text{CLS}]}$ , yielding the image representation  $\mathbf{v}$  in the cross-modal shared space.

**2) Text Encoder  $En_t(\cdot)$ .** Following [22], we employ soft prompt tuning, making prompts tokens better adapted to CZSL. Specifically, we formulate the prompt as a set comprising prefix context and category representations. By converting the prompt into learnable embeddings, we provide the model with the flexibility to adapt its language-based observation. The prompts of state, object, and composition, denoted as  $\mathbf{P}_s$ ,  $\mathbf{P}_o$ , and  $\mathbf{P}_c$ , are formulated as:

$$\begin{aligned} \mathbf{P}_s &= [\mathbf{x}_0; \mathbf{x}_1; \dots; \mathbf{x}_M; \mathbf{x}_s; \mathbf{o}], \\ \mathbf{P}_o &= [\mathbf{x}_0; \mathbf{x}_1; \dots; \mathbf{x}_M; \mathbf{x}_o], \\ \mathbf{P}_c &= [\mathbf{x}_0; \mathbf{x}_1; \dots; \mathbf{x}_M; \mathbf{x}_s; \mathbf{x}_o], \end{aligned} \quad (1)$$

where  $[\mathbf{x}_0; \dots; \mathbf{x}_M]$  represents the prefix context with the word embedding of “a photo of” as an initialization,  $\mathbf{x}_s$  and  $\mathbf{x}_o$  represent word embedding of the state and object categories,  $\mathbf{o}$  represents word embedding of the word “object”. The context length is denoted by  $M$ . Similar to the token representation in the visual part, textual prompts

<sup>1</sup>The detailed descriptions of the PEFT strategies are left in Appendix.

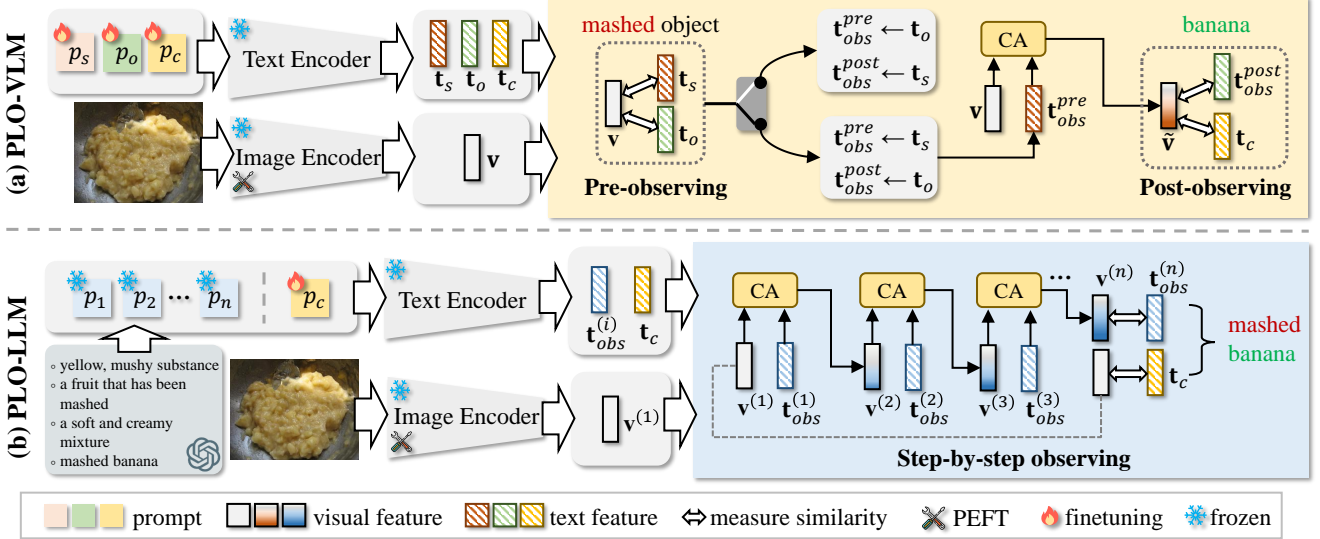


Figure 2. (a) **PLO-VLM**: A two-step approach using a pre-observing classifier to dynamically determine the first observation. (b) **PLO-LLM**: A multi-step approach that observes composition-specific prompts from LLMs step-by-step.

are then converted to learnable embeddings and fed into the text encoder  $En_t(\cdot)$  to update the patch tokens  $\mathcal{T} = \{\mathbf{t}_{[\text{CLS}]}, \mathbf{t}_1, \mathbf{t}_2, \dots, \mathbf{t}_M\}$  with self-attention blocks. Subsequently, the output  $\hat{\mathbf{t}}_{[\text{CLS}]}$  of the three types of prompts are fed into a single linear layer to project them as text representations  $\mathbf{t}_s$ ,  $\mathbf{t}_o$ , and  $\mathbf{t}_c$ .

Text representations  $\mathbf{t}_s$ ,  $\mathbf{t}_o$ , and  $\mathbf{t}_c$  and image representation  $\mathbf{v}$  are then used in the subsequent steps of PLO-VLM and PLO-LLM process for compositional classification.

### 3.2. PLO-VLM

As illustrated in Figure 2(a), PLO-VLM adopts a dynamic two-step observation framework to decide whether to prioritize observing the state or object primitive. Next, the prompt features of the selected primitive are integrated into the image using cross-modal attention (CA), which highlights regions of interest related to the observation. By further comparing the similarities between the refined image features and the text features of the remaining primitives, PLO-VLM effectively recognizes state-object compositions.

**1) Pre-observing.** The pre-observing classifier recognizes the first primitive by measuring the cosine similarity  $\mathcal{S}(\cdot, \cdot)$  between the image representation  $\mathbf{v}$  and the text representations of the state primitive  $\mathbf{t}_s$  and the object primitive  $\mathbf{t}_o$ :

$$\mathcal{F}_{obs}^{pre}(\mathbf{v}, \mathbf{t}_s, \mathbf{t}_o) = \mathcal{S}(\mathbf{v}, \mathbf{t}_s) \oplus \mathcal{S}(\mathbf{v}, \mathbf{t}_o), \quad (2)$$

where  $\oplus$  denotes concatenation. The first observation is the prompt of  $\text{argmax}(\mathcal{F}_{obs}^{pre}(\cdot))$ . Its corresponding text representation is  $\mathbf{t}_{obs}^{pre}$ . For instance in Figure 2(a), the first observation is the prompt of the state “mashed object”, and  $\mathbf{t}_{obs}^{pre}$  will correspond to the text representation  $\mathbf{t}_s$ .

**2) Post-observing.** After obtaining the first observation, we

employ learnable residual cross-modal attention modules to extract the interest features of the first observation for refined image representations  $\tilde{\mathbf{v}}$ , which are widely adopted in existing methods [3, 10, 22]. The CA module is defined as:

$$\text{CA}(\mathbf{q}, \mathbf{K}, \mathbf{V}) = \mathbf{q} + \text{FFN}(\text{LN}(\mathbf{q} + \text{MHA}(\mathbf{q}, \mathbf{K}, \mathbf{V}))), \quad (3)$$

where  $\mathbf{q}$ ,  $\mathbf{K}$ , and  $\mathbf{V}$  are the features of query, key, and value, respectively. The module FFN, LN, and MHA are feed-forward networks, layer normalization, and multi-head attention, respectively. The refined image representations  $\tilde{\mathbf{v}}$  are derived based on the first observation as follows:

$$\tilde{\mathbf{V}} = \text{CA}(\mathcal{V}, \mathcal{T}_{obs}^{pre}, \mathcal{T}_{obs}^{pre}), \tilde{\mathbf{v}} = \text{FC}(\tilde{\mathbf{V}}), \quad (4)$$

where  $\mathcal{T}_{obs}^{pre}$  is the output patch tokens of the prompt corresponding to  $\mathbf{t}_{obs}^{pre}$ . The [CLS] token of  $\tilde{\mathbf{V}}$  is then fed into a linear layer to obtain the refined image representation  $\tilde{\mathbf{v}}$ . The refined image representation is utilized to calculate the similarity between the prompt of retain primitive, e.g., object “banana” in Figure 2(a), written as:

$$\begin{aligned} p(s|I) &= \pi(\mathcal{S}(\tilde{\mathbf{v}}, \mathbf{t}_{obs}^{post}), \tau), \text{ if } \mathbf{t}_{obs}^{post} \leftarrow \mathbf{t}_s, \\ p(o|I) &= \pi(\mathcal{S}(\tilde{\mathbf{v}}, \mathbf{t}_{obs}^{post}), \tau), \text{ if } \mathbf{t}_{obs}^{post} \leftarrow \mathbf{t}_o. \end{aligned} \quad (5)$$

where  $\pi(\cdot)$  is the softmax function and  $\tau$  denotes the temperature hyper-parameter. The  $\mathbf{t}_{obs}^{post}$  represents the text presentation of the prompt of retaining state or object primitive, respectively. Additionally, to ensure that the refined feature encompasses both state and object features, we also compare its similarity with the text presentations of the composition prompt, which is defined as follows:

$$p(c|I) = \pi(\mathcal{S}(\tilde{\mathbf{v}}, \mathbf{t}_c), \tau), \quad (6)$$

where the  $\mathbf{t}_c$  corresponds to the text representation of the



prompt of the composition category.

### 3.3. PLO-LLM

As shown in Figure 2(b), it employs a multi-step observation process and starts by generating a sequence of observation prompts for each composition category using an LLM, *i.e.*, GPT [4]. Then, the final compositional classification is determined by observing step by step whether observation prompts exist in the image.

**1) Observation Prompts Generation.** To elaborate, for each composition category  $c \in C$ , a sequence of the observation hard prompts  $\mathcal{P}_c = \{\mathbf{P}_c^{(i)}\}_{i=1}^n$  is generated using an LLM with the designed prompt (refer to the Appendix), where  $n$  denotes the number of observation steps. Note that these prompts are frozen. For instance, in Figure 2(b), the observation prompts are listed in the blue box, *e.g.*, “yellow, mushy substance” for “mashed banana”.

**2) Step-by-step Observing.** At each observation step  $i$ , the image representation  $\mathbf{v}^{(i)}$  and the text representation of the current observation prompt  $\mathbf{t}_{obs}^{(i)}$  are fed into the learnable CA module. The CA module updates the image representation to produce the refined image representation  $\tilde{\mathbf{v}}^{(i)}$ :

$$\begin{aligned}\tilde{\mathbf{v}}^{(i)} &= \text{CA}(\mathcal{V}^{(i)}, \mathcal{T}_{obs}^{(i)}, \mathcal{T}_{obs}^{(i)}), \\ \mathbf{v}^{(i+1)} &= \tilde{\mathbf{v}}^{(i)} = \text{FC}(\tilde{\mathbf{v}}^{(i)}),\end{aligned}\quad (7)$$

where  $\tilde{\mathbf{v}}^{(i)}$  incorporates information from the current observation prompt, which is then utilized in the next observation step to calculate the similarity between the image and the next observation prompt  $\mathbf{t}_{obs}^{(i+1)}$ . This process is repeated for all observation steps, iteratively updating the image representation with information from each observation prompt. The result of each observation is  $\mathcal{S}(\mathbf{v}^{(i)}, \mathbf{t}_{obs}^{(i)})$ .

Since each observation is conditioned on the previous step, the probability of each step is given by:

$$p(c^{(i)}|I, c^{(1)}, \dots, c^{(i-1)}) = \pi(\mathcal{S}(\mathbf{v}^{(i)}, \mathbf{t}_{obs}^{(i)}), \tau). \quad (8)$$

Furthermore, to facilitate the model in learning semantic representations suitable for CZSL without being solely influenced by hard prompts, we also incorporate the similarity between the original image representation  $\mathbf{v}$  and the text representation  $\mathbf{t}_c$  of the learnable composition soft prompts to aid in prediction. The probability is calculated as follows:

$$p^{Soft}(c|I) = \pi(\mathcal{S}(\mathbf{v}, \mathbf{t}_c), \tau). \quad (9)$$

### 3.4. Training Objectives and Inference

**PLO-VLM.** During training, we employ four main losses to optimize the model: multi-label loss  $\mathcal{L}_{obs}$  for the pre-observing classifier and cross-entropy losses  $\mathcal{L}_s$ ,  $\mathcal{L}_o$ , and  $\mathcal{L}_c$  for state, object, and composition, respectively. The combined loss is formulated as:

$$\mathcal{L}_{PLO}^{VLM} = \mathcal{L}_{obs} + \mathcal{L}_s + \mathcal{L}_o + \mathcal{L}_c. \quad (10)$$

The multi-label loss optimizes the pre-observing classifier, responsible for predicting whether to initially observe the state or object primitive in the input image. It is calculated using binary cross-entropy loss for each target label:

$$\begin{aligned}\mathcal{L}_{obs} &= -y_{obs} \log(\sigma(\mathcal{F}_{obs}^{pre})) \\ &\quad + (1 - y_{obs}) \log(1 - \sigma(\mathcal{F}_{obs}^{pre})),\end{aligned}\quad (11)$$

where  $\sigma(\cdot)$  denotes the sigmoid function.  $y_{obs} = [y_s, y_o]$  is the ground-truth multi-label target for the pre-observing classifier, where  $y_s$  and  $y_o$  are binary values of ground-truth state and object categories, respectively.

The optimization of classification involves three independent cross-entropy losses:  $\mathcal{L}_s$  for state,  $\mathcal{L}_o$  for object, and  $\mathcal{L}_c$  for composition. Taking the state classification as an illustrative example, its loss  $\mathcal{L}_s$  is defined as:

$$\mathcal{L}_s = -\sum_S y_s \log(p(s|I)). \quad (12)$$

During inference, we pick the composition with the highest score of  $p(c|I)$  as our predicted label for the input image.

**PLO-LLM.** In the training of PLO-LLM, the loss includes the cross-entropy loss  $\mathcal{L}_{step}$  for each observation step and cross-entropy loss  $\mathcal{L}_c$  for composition:

$$\mathcal{L}_{PLO}^{LLM} = \mathcal{L}_{step} + \mathcal{L}_c, \quad (13)$$

$\mathcal{L}_c$  is the same as in PLO-VLM, and  $\mathcal{L}_{step}$  is calculated by:

$$\mathcal{L}_{step} = -\sum_{i=1}^n \sum_{j \in C} y_c^{(i)} \log(p(c_j^{(i)}|I, c_j^{(1)}, \dots, c_j^{(i-1)})), \quad (14)$$

where  $y_c^{(i)}$  is the ground truth one-hot encoded composition label for the  $i$ -th observation prompt at step  $i$ .

Since PLO-LLM includes both the step-by-step hard prompt observation and soft prompt during training, the inference process involves predicting the composition label  $\hat{y}_c$  by calculating the probabilities of the composition categories using the following equations:

$$\begin{aligned}p(c|I) &= p^{Soft}(c|I) + p^{Hard}(c|I), \\ p^{Hard}(c|I) &= \prod_{i=1}^n p(c^{(i)}|I, c^{(1)}, \dots, c^{(i-1)}),\end{aligned}\quad (15)$$

where  $p(c|I)$  is the probability of composition category  $c$ ,  $p^{Soft}(c|I)$  is the probability based on soft prompts, and  $p^{Hard}(c|I)$  is based on hard prompts at each observing step. The composition category with the highest overall probability is chosen as the final predicted composition label  $\hat{y}_c$ .

The training and inference procedures of PLO-VLM and PLO-LLM are shown in the Appendix.

## 4. Experiments

### 4.1. Experiment Settings

**Datasets.** We evaluate performance on three challenging benchmarks: **MIT-States** [12]: It comprises 53,753 natural

Setting	Method		MIT-States				UT-Zappos				C-GQA			
			S	U	HM	AUC	S	U	HM	AUC	S	U	HM	AUC
Closed-World	CLIP [34]	ICML'21	30.2	46.0	26.1	11.0	15.8	49.1	15.6	5.0	7.5	25.0	8.6	1.4
	CoOp [43]	IJCV'22	34.4	47.6	29.8	13.5	52.1	49.3	34.6	18.8	20.5	26.8	17.1	4.4
	Co-CGE [26]	TPAMI'22	46.7	45.9	33.1	17.0	63.4	71.3	49.7	36.3	34.1	21.2	18.9	5.7
	ProDA [24]	CVPR'22	37.4	51.7	32.7	16.1	63.7	60.7	47.6	32.7	-	-	-	-
	PromptCompVL [24]	arXiv'22	48.5	47.2	35.3	18.3	64.4	64.0	46.1	32.2	-	-	-	-
	CSP [30]	ICLR'23	46.6	49.9	36.3	19.4	64.2	66.2	46.6	33.0	28.8	26.8	20.5	6.2
	DFSP(i2t) [22]	CVPR'23	47.4	52.4	37.2	20.7	64.2	66.4	45.1	32.1	35.6	29.3	24.3	8.7
	DFSP(BiF) [22]	CVPR'23	47.1	52.8	37.7	20.8	63.3	69.2	47.1	33.5	36.5	32.0	26.2	9.9
	DFSP(t2i) [22]	CVPR'23	46.9	52.0	37.3	20.6	66.7	71.7	47.2	36.0	38.2	32.0	27.1	10.5
	Troika [10]	arXiv'23	49.0	53.0	<b>39.3</b>	22.1	66.8	73.8	54.6	41.7	41.0	35.7	29.4	12.4
	PLID [3]	arXiv'23	<b>49.7</b>	52.4	39.0	22.1	67.3	68.8	52.4	38.7	38.8	33.0	27.9	11.0
	GIPCOL [38]	WACV'24	48.5	49.6	36.6	19.9	65.0	68.5	48.8	36.2	31.9	28.4	22.5	7.1
	<b>PLO-VLM (Ours)</b>		49.6	52.7	39.0	<b>22.2</b>	67.8	<b>75.6</b>	53.1	<b>42.0</b>	43.9	<b>38.2</b>	<b>32.2</b>	<b>14.5</b>
	<b>PLO-LLM (Ours)</b>		49.6	<b>53.2</b>	39.0	21.9	<b>68.3</b>	73.0	<b>54.8</b>	41.6	<b>44.3</b>	37.9	31.2	14.3
Open-World	CLIP [34]	ICML'21	30.1	14.3	12.8	3.0	15.7	20.6	11.2	2.2	7.5	4.6	4.0	0.3
	CoOp [43]	IJCV'22	34.6	9.3	12.3	2.8	52.1	31.5	28.9	13.2	21.0	4.6	5.5	0.7
	Co-CGE [26]	TPAMI'22	38.1	20.0	17.7	5.6	59.9	56.2	45.3	28.4	33.2	3.9	5.3	0.9
	ProDA [24]	CVPR'22	37.5	18.3	17.3	5.1	63.9	34.6	34.3	18.4	-	-	-	-
	PromptCompVL [24]	arXiv'22	48.5	16.0	17.7	6.1	64.6	44.0	37.1	21.6	-	-	-	-
	CSP [30]	ICLR'23	46.3	15.7	17.4	5.7	64.1	44.1	38.9	22.7	28.7	5.2	6.9	1.2
	DFSP(i2t) [22]	CVPR'23	47.2	18.2	19.1	6.7	64.3	53.8	41.2	26.4	35.6	6.5	9.0	2.0
	DFSP(BiF) [22]	CVPR'23	47.1	18.1	19.2	6.7	63.5	57.2	42.7	27.6	36.4	7.6	10.6	2.4
	DFSP(t2i) [22]	CVPR'23	47.5	18.5	19.3	6.8	66.8	60.0	44.0	30.3	38.3	7.2	10.4	2.4
	Troika [10]	arXiv'23	48.8	18.7	20.1	7.2	66.4	61.2	47.8	33.0	40.8	7.9	10.9	2.7
	PLID [3]	arXiv'23	49.1	18.7	20.0	7.3	67.6	55.5	46.6	30.8	39.1	7.5	10.6	2.5
	GIPCOL [38]	WACV'24	48.5	16.0	17.9	6.3	65.0	45.0	40.1	23.5	31.6	5.5	7.3	1.3
	<b>PLO-VLM (Ours)</b>		<b>49.5</b>	<b>18.7</b>	<b>20.5</b>	<b>7.4</b>	<b>68.0</b>	<b>63.5</b>	<b>47.8</b>	<b>33.1</b>	<b>43.9</b>	<b>10.4</b>	<b>13.9</b>	<b>3.9</b>

Table 1. Performance (%) of state-of-the-art CZSL models on three datasets in closed-world and open-world settings.

images, with 115 states and 245 objects. In the closed-world setting, the search space includes 1,262 seen compositions and 300/400 unseen compositions for validation/testing. 2) **UT-Zappos** [29]: It consists of 50,025 images of shoes, with 16 states and 12 objects. In the closed-world experiments, we considered 83 seen compositions and 15/18 (validation/test) unseen compositions following the constraints defined in [33]. 3) **C-GQA** [39]: It contains 453 states and 870 objects, comprising a total of 39,298 images. The dataset is divided into 5,592 seen compositions for training, and 1,040/923 unseen compositions for validation/testing, respectively. In the open-world settings, these datasets contain 28,175, 192, and 278,362 compositions, respectively.

**Metrics.** We followed the established CZSL evaluation protocol [25] and assessed all results using four metrics in both closed-world and open-world scenarios: 1) *Seen (S)*: This metric measures the accuracy specifically for seen compositions. 2) *Unseen (U)*: It evaluates the accuracy exclusively for unseen compositions. 3) *Harmonic Mean (HM)*: The best harmonic mean between the seen and unseen accuracy is calculated, providing a comprehensive performance measure. 4) *Area Under the Curve (AUC)*: This metric computes the area under the seen-unseen accuracy curve, capturing the overall performance characteristics over a wide

range of operating points from  $-\infty$  to  $+\infty$ .

**Implementation Details.** Please refer to the appendix.

## 4.2. Comparison with the State-of-the-Arts

**Setting.** To ensure fair comparisons with existing work, we conducted a comparative analysis of PLO against several CLIP-based approaches that use the same backbone (ViT-L/14). The methods including **CLIP** [34], **CoOp** [43], **Co-CGE** [26], **ProDA** [24], **PromptCompVL** [37], **CSP** [30], all versions of **DFSP** [22], **Troika** [10], **PLID** [3], and **GIPCOL** [38]. The results are shown in Table 1<sup>2</sup>.

**Quantitative Analysis.** It can be seen that PLO outperforms nearly all competitors by clear margins in both closed-world and open-world settings across three prevalent benchmarks. In the closed-world setting: 1) PLO-VLM surpasses the leading competitor, Troika, by **0.1%**, **0.3%**, and **2.1%** in AUC (the core metric) on the MIT-States, UT-Zappos, and C-GQA datasets, respectively. 2) PLO-VLM and PLO-LLM achieve dominant results on C-GQA (the most challenging dataset), with HM scores of **32.2%** and **31.2%**, compared to Troika’s 29.4%. In the open-world

<sup>2</sup>To limit the money spent on generating prompts with GPT, we only reported the results of PLO-LLM in the closed-world setting.

Method	C-GQA Cross-Domain			
	S	U	HM	AUC
DFSP [22]	49.2	28.4	26.6	11.7
PLO-VLM	50.8	28.7	28.7	12.5
PLO-LLM	52.5	32.1	32.9	15.1

Table 2. The cross-domain evaluation on C-GQA dataset.

Component		MIT-States			
PEFT	DO	S	U	HM	AUC
✗	✗	47.6	51.2	36.9	20.4
✓	✗	47.7	52.8	38.1	21.3
✗	✓	48.5	52.0	38.3	21.3
✓	✓	49.6	52.7	39.0	22.2

Table 3. Ablation study on each component in PLO-VLM. **PEFT**: It adopts the parameter efficient fine-tuning in the image encoder. **DO**: It utilizes the dynamic observation strategy.

First Observation	MIT-States			
	S	U	HM	AUC
Baseline	47.6	51.2	36.9	20.4
State	49.5	52.0	39.0	21.9
Object	48.4	52.8	38.2	21.5
Dynamic	49.6	52.7	39.0	22.2

Table 4. Ablation study on observation order in PLO-VLM.

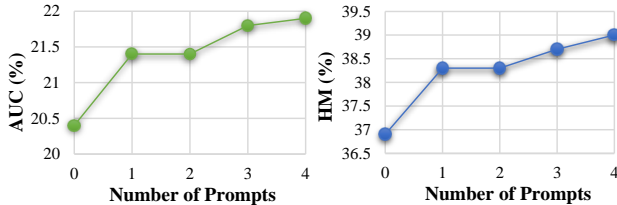


Figure 3. Ablation study on the different number of observation prompts in PLO-LLM.

setting<sup>2</sup>, PLO-VLM attains the highest AUC across all three datasets, with scores of **7.4%**, **33.1%**, and **3.9%**. These numerical results substantiate our motivation of empowering models with the *observing* capabilities to understand visual compositions in a simple to complex manner, rather than modeling each composition separately.

### 4.3. Cross-Domain Evaluation

**Setting.** For a more comprehensive evaluation, we trained DFSP(i2t) [22], PLO-VLM and PLO-LLM on the MIT-States dataset and tested cross-domain performance on the C-GQA dataset, selecting categories that correspond to the states and objects in MIT-States for a consistent assessment.

**Results.** As shown in Table 2, PLO-LLM exhibits superior performance on C-GQA dataset, particularly in the accuracy of unseen categories (32.1% vs. 28.7%) and consistently outperforms in HM and AUC scores. This enhancement stems from the GPT-generated sequence of observations in PLO-LLM, which operates independently of the visual modality, thereby bolstering cross-domain robustness.

Backbone	Method	MIT-States			
		S	U	HM	AUC
ViT-B/32	DFSP [22]	36.7	43.4	29.4	13.2
	PLO-VLM	41.1	44.2	31.3	14.8
	PLO-LLM	44.2	47.9	34.3	17.4
ViT-B/16	DFSP [22]	39.6	46.5	31.5	15.1
	PLO-VLM	43.9	46.6	34.1	17.0
	PLO-LLM	41.2	44.7	31.4	14.8
ViT-L/14	DFSP [22]	46.9	52.0	37.3	20.6
	PLO-VLM	49.6	52.7	39.0	22.2
	PLO-LLM	49.6	53.2	39.0	21.9

Table 5. Ablation study on different CLIP backbones.

### 4.4. Ablation Study

In this section, we conducted ablation studies to analyze the effectiveness of each component in PLO-VLM, the impact of the observation order in PLO-VLM, the number of observation prompts in PLO-LLM, and the network architectures of the based CLIP. All experiments were conducted on the MIT-States dataset under the closed-world setting.

**Effectiveness of Each Component in PLO-VLM.** The contribution of Parameter Efficient Fine-Tuning (PEFT)<sup>1</sup> and Dynamic Observation (DO) strategies to PLO-VLM was assessed, as summarized in Table 3. Our analysis can yield the following insights: 1) **PEFT (Fine-Tuning in  $En_v$ )**: Incorporating PEFT into the image encoder  $En_v$  marginally improves HM metric, with an increase from 36.9% to 38.1%. This improvement underscores the subtle yet impactful role of fine-tuning the encoder’s lightweight layers. Extra experimental results of PEFT are left in the **appendix**. 2) **DO**: Implementing DO in isolation enhances the model’s ability to recognize both seen and unseen compositions, as reflected in a boost of the seen metric from 47.6% to 48.5% and unseen metric from 51.2% to 52.0%. This highlights the critical impact of dynamically determining observations in understanding visual compositions. 3) **Synergistic Impact of PEFT and DO**: When PEFT and DO are synergistically applied, they collectively achieve the highest AUC of 22.2%. This composite application underlines the effectiveness of integrating both strategies, leading to optimal model performance in recognizing compositions.

**Observation Order.** We explored the influence of different observation orders in PLO-VLM by using various strategies for determining the first observation: predicting the state primitive first, predicting the object primitive first, and dynamically deciding the observation order. From Table 4, we can observe: 1) The multi-step observation leads to significant performance gains against the baseline across all the metrics. 2) Dynamically deciding the observation order based on the input image yields the highest overall performance. These findings demonstrated the effectiveness of adaptively choosing the most informative observation step based on the content of the input image, which is of impor-








	Success Cases					Failure Cases	
Image							
GT	mashed, potato	pressed, candy	old, toy	ruffled, bag	moldy, orange	bent, blade	muddy, river
$K = 1$	mashed, potato	pressed, candy	old, toy	ruffled, bag	moldy, orange	rusty, knife	muddy, stream
$K = 2$	mashed, garlic	chipped, candy	painted, toy	ruffled, fabric	moldy, fruit	bent, knife	muddy, canyon
$K = 3$	crushed, potato	sliced, candy	filled, toy	ruffled, basket	moldy, tomato	bent, blade	muddy, river

Figure 4. Top- $K$  predictions on for randomly selected cases from MIT-States. The top and bottom rows show the results of open-world settings, respectively. Correct and incorrect predictions are highlighted in green and red, respectively.

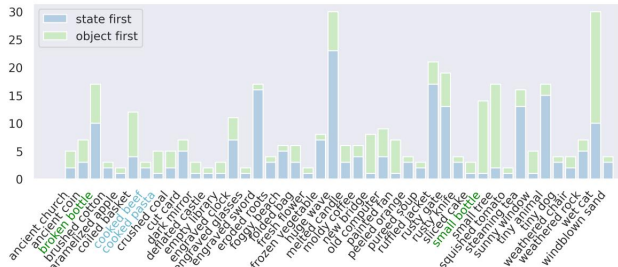


Figure 5. Distribution of samples where state or object is first observed in PLO-VLM on the test set of MIT-States.




Image			
GT	mashed, potato	burnt, coal	crumpled, leaf
w/o obs	mashed, garlic	burnt, leaf	burnt, leaf
pre-obs	mashed object	burnt object	leaf
with obs	mashed, potato	burnt, coal	crumple, leaf

Figure 6. Top-1 predictions of PLO-VLM with and without dynamically observing under the open-world setting on MIT-States dataset. Pre-observing primitives are highlighted in blue.

tance due to the conditioned variance nature of CZSL.

Figure 5 reveals the dynamic observation strategy of PLO-VLM, which selects states or objects first based on their visual saliency in a composition<sup>3</sup>. The “cooked pasta” often undergoes object-first observations owing to its distinct visuals, whereas “broken bottle” typically requires state-first recognition due to the impactful visual change presented by the state “broken”. PLO-VLM’s context-aware approach mirrors human cognition in compositional zero-shot learning, leading to more precise recognition. Furthermore, we visualized top-1 predictions of PLO-VLM with and without dynamically observing in Figure 6. In a sense, the pre-observed primitive can represent a more prominent feature in the image (e.g., “mashed object” and “burnt object”). By virtue of pre-observed primitive, PLO-VLM consistently achieved accurate predictions.

<sup>3</sup>More visualization results are left in the appendix.

**Number of Observation Prompts.** We investigated the impact of the number of observation prompts in PLO-LLM. We varied the number of prompts for each composition category and evaluated the model’s performance accordingly. The results, depicted in Figure 3, reveal a nuanced relationship between the number of prompts and the model’s accuracy. As expected, increasing the number of observation prompts can generally lead to improved performance.

**Effect of Network Architectures.** We further examined the influence of replacing CLIP backbones in our PLO-VLM and PLO-LLM. All results are reported in Table 5. Those consistent performance gains compared to the previous SOTA reaffirmed the efficacy and robustness of the proposed methodology. We chose ViT-L/14 by default.

**Qualitative Results.** We provided top- $K$  predictions of PLO-VLM in the open-world settings in Figure 4. Our progressive observation strategy enables a thorough grasp of compositions, which is particularly effective in recognizing unseen compositions by bridging the gap between base and novel categories. Notably, even when our model’s top-1 prediction is not exactly matched, it still accurately predicts the state primitive, and the object primitive also appears to be reasonable (e.g., muddy stream). These results underscore PLO’s effectiveness in capturing pertinent visual cues and enabling comprehensive composition understanding.

## 5. Conclusion

In this paper, we presented PLO, a novel solution for addressing the challenges of conditioned variance in CZSL. Unlike existing methods modeling each composition separately, PLO effectively captures the interactions between state and object primitives by dynamically determining the observation order, leading to a holistic understanding of visual concepts for each composition. The two variants, PLO-VLM and PLO-LLM, harness the power of VLMs and LLMs to refine image representations in a simple to complex manner. Experimental results on three gold-standard CZSL benchmarks demonstrated their superiority over existing frameworks. PLO opens a new avenue for CZSL from the perspective of endowing models with *observing* capabilities, and we hope it will pave the way for future research.



## References

- [1] Jean-Baptiste Alayrac, Jeff Donahue, Pauline Luc, Antoine Miech, Iain Barr, Yana Hasson, Karel Lenc, Arthur Mensch, Katherine Millican, Malcolm Reynolds, et al. Flamingo: a visual language model for few-shot learning. In *NIPS*, pages 23716–23736, 2022. 3
- [2] Muhammad Umer Anwaar, Zhihui Pan, and Martin Kleins-teuber. On leveraging variational graph embeddings for open world compositional zero-shot learning. In *ACM MM*, pages 4645–4654, 2022. 2
- [3] Wentao Bao, Lichang Chen, Heng Huang, and Yu Kong. Prompting language-informed distribution for compositional zero-shot learning. *arXiv preprint arXiv:2305.14428*, 2023. 4, 6
- [4] Tom Brown, Benjamin Mann, Nick Ryder, Melanie Subbiah, Jared D Kaplan, Prafulla Dhariwal, Arvind Neelakan-tan, Pranav Shyam, Girish Sastry, Amanda Askell, et al. Lan-guage models are few-shot learners. In *NIPS*, pages 1877–1901, 2020. 2, 5
- [5] Shaozhe Hao, Kai Han, and Kwan-Yee K Wong. Learning attention as disentangler for compositional zero-shot learn-ing. In *CVPR*, pages 15315–15324, 2023. 2
- [6] Neil Houlsby, Andrei Giurgiu, Stanislaw Jastrzebski, Bruna Morrone, Quentin De Laroussilhe, Andrea Gesmundo, Mona Attariyan, and Sylvain Gelly. Parameter-efficient transfer learning for nlp. In *ICML*, pages 2790–2799. PMLR, 2019. 3, 2
- [7] Edward J Hu, Yelong Shen, Phillip Wallis, Zeyuan Allen-Zhu, Yuanzhi Li, Shean Wang, Lu Wang, and Weizhu Chen. LoRA: Low-rank adaptation of large language models. In *ICLR*, 2022. 3, 2
- [8] Xiaoming Hu and Zilei Wang. Leveraging sub-class discrim-ination for compositional zero-shot learning. In *AAAI*, pages 890–898, 2023. 2
- [9] Yushi Hu, Hang Hua, Zhengyuan Yang, Weijia Shi, Noah A Smith, and Jiebo Luo. Promptcap: Prompt-guided task-aware image captioning. *arXiv preprint arXiv:2211.09699*, 2022. 3
- [10] Siteng Huang, Biao Gong, Yutong Feng, Yiliang Lv, and Donglin Wang. Troika: Multi-path cross-modal trac-tion for compositional zero-shot learning. *arXiv preprint arXiv:2303.15230*, 2023. 2, 3, 4, 6
- [11] Fushuo Huo, Wenchao Xu, Song Guo, Jingcai Guo, Haozhao Wang, and Ziming Liu. Procc: Progressive cross-primitive consistency for open-world compositional zero-shot learn-ing. *arXiv preprint arXiv:2211.12417*, 2022. 2
- [12] Phillip Isola, Joseph J Lim, and Edward H Adelson. Dis-covering states and transformations in image collections. In *CVPR*, pages 1383–1391, 2015. 2, 5
- [13] Shyamgopal Karthik, Massimiliano Mancini, and Zeynep Akata. Kg-sp: Knowledge guided simple primitives for open world compositional zero-shot learning. In *CVPR*, pages 9336–9345, 2022. 2
- [14] Muhammad Gul Zain Ali Khan, Muhammad Ferjad Naeem, Luc Van Gool, Alain Pagani, Didier Stricker, and Muham-mad Zeshan Afzal. Learning attention propagation for com-positional zero-shot learning. In *WACV*, pages 3828–3837, 2023. 2
- [15] Hanjae Kim, Jiyoung Lee, Seongheon Park, and Kwanghoon Sohn. Hierarchical visual primitive experts for composi-tional zero-shot learning. *ICCV*, 2023. 2
- [16] Takeshi Kojima, Shixiang Shane Gu, Machel Reid, Yutaka Matsuo, and Yusuke Iwasawa. Large language models are zero-shot reasoners. In *NeurIPS*, 2022. 2
- [17] Junnan Li, Dongxu Li, Caiming Xiong, and Steven Hoi. Blip: Bootstrapping language-image pre-training for unified vision-language understanding and generation. In *ICML*, pages 12888–12900. PMLR, 2022. 3
- [18] Lin Li, Jun Xiao, Guikun Chen, Jian Shao, Yueting Zhuang, and Long Chen. Zero-shot visual relation detection via composite visual cues from large language models. *arXiv preprint arXiv:2305.12476*, 2023. 3
- [19] Xiangyu Li, Xu Yang, Kun Wei, Cheng Deng, and Muli Yang. Siamese contrastive embedding network for composi-tional zero-shot learning. In *CVPR*, pages 9326–9335, 2022. 1, 2
- [20] Yong-Lu Li, Yue Xu, Xiaohan Mao, and Cewu Lu. Sym-metry and group in attribute-object compositions. In *CVPR*, pages 11316–11325, 2020. 2
- [21] Jiachang Liu, Dinghan Shen, Yizhe Zhang, Bill Dolan, Lawrence Carin, and Weizhu Chen. What makes good in-context examples for gpt-3? *arXiv preprint arXiv:2101.06804*, 2021. 2
- [22] Xiaocheng Lu, Song Guo, Ziming Liu, and Jingcai Guo. De-composed soft prompt guided fusion enhancing for compo-sitional zero-shot learning. In *CVPR*, pages 23560–23569, 2023. 2, 3, 4, 6, 7
- [23] Xiaocheng Lu, Ziming Liu, Song Guo, Jingcai Guo, Fushuo Huo, Sikai Bai, and Tao Han. Drpt: Disentangled and re-current prompt tuning for compositional zero-shot learning. *arXiv preprint arXiv:2305.01239*, 2023. 2
- [24] Yuning Lu, Jianzhuang Liu, Yonggang Zhang, Yajing Liu, and Xinmei Tian. Prompt distribution learning. In *CVPR*, pages 5206–5215, 2022. 6
- [25] Massimiliano Mancini, Muhammad Ferjad Naeem, Yongqin Xian, and Zeynep Akata. Open world compositional zero-shot learning. In *CVPR*, pages 5222–5230, 2021. 1, 6
- [26] Massimiliano Mancini, Muhammad Ferjad Naeem, Yongqin Xian, and Zeynep Akata. Learning graph embeddings for open world compositional zero-shot learning. *TPAMI*, 2022. 2, 6
- [27] Sachit Menon and Carl Vondrick. Visual classification via description from large language models. In *ICLR*, 2023. 3
- [28] Ishan Misra, Abhinav Gupta, and Martial Hebert. From red wine to red tomato: Composition with context. In *CVPR*, pages 1792–1801, 2017. 2
- [29] Muhammad Ferjad Naeem, Yongqin Xian, Federico Tombari, and Zeynep Akata. Learning graph embeddings for compositional zero-shot learning. In *CVPR*, pages 953–962, 2021. 1, 2, 6
- [30] Nihal V Nayak, Peilin Yu, and Stephen H Bach. Learning to compose soft prompts for compositional zero-shot learning. *ICLR*, 2023. 2, 6

- [31] Zachary Novack, Julian McAuley, Zachary Chase Lipton, and Saurabh Garg. Chils: Zero-shot image classification with hierarchical label sets. In *ICML*, pages 26342–26362. PMLR, 2023. 3
- [32] Adam Paszke, Sam Gross, Francisco Massa, Adam Lerer, James Bradbury, Gregory Chanan, Trevor Killeen, Zeming Lin, Natalia Gimelshein, Luca Antiga, Alban Desmaison, Andreas Kopf, Edward Yang, Zachary DeVito, Martin Raison, Alykhan Tejani, Sasank Chilamkurthy, Benoit Steiner, Lu Fang, Junjie Bai, and Soumith Chintala. Pytorch: An imperative style, high-performance deep learning library. In *Advances in Neural Information Processing Systems*. Curran Associates, Inc., 2019. 2
- [33] Senthil Purushwalkam, Maximilian Nickel, Abhinav Gupta, and Marc’Aurelio Ranzato. Task-driven modular networks for zero-shot compositional learning. In *ICCV*, pages 3593–3602, 2019. 2, 6
- [34] Alec Radford, Jong Wook Kim, Chris Hallacy, Aditya Ramesh, Gabriel Goh, Sandhini Agarwal, Girish Sastry, Amanda Askell, Pamela Mishkin, Jack Clark, et al. Learning transferable visual models from natural language supervision. In *ICML*, pages 8748–8763. PMLR, 2021. 2, 3, 6
- [35] Maria Tsimpoukelli, Jacob L Menick, Serkan Cabi, SM Eslami, Oriol Vinyals, and Felix Hill. Multimodal few-shot learning with frozen language models. In *NIPS*, pages 200–212, 2021. 3
- [36] Qingsheng Wang, Lingqiao Liu, Chenchen Jing, Hao Chen, Guoqiang Liang, Peng Wang, and Chunhua Shen. Learning conditional attributes for compositional zero-shot learning. In *CVPR*, pages 11197–11206, 2023. 2
- [37] Guanyue Xu, Parisa Kordjamshidi, and Joyce Chai. Prompting large pre-trained vision-language models for compositional concept learning. *arXiv preprint arXiv:2211.05077*, 2022. 6
- [38] Guanyue Xu, Joyce Chai, and Parisa Kordjamshidi. Gipcol: Graph-injected soft prompting for compositional zero-shot learning. *WACV*, 2023. 6
- [39] Aron Yu and Kristen Grauman. Fine-grained visual comparisons with local learning. In *CVPR*, pages 192–199, 2014. 2, 6
- [40] Tian Zhang, Kongming Liang, Ruoyi Du, Xian Sun, Zhanyu Ma, and Jun Guo. Learning invariant visual representations for compositional zero-shot learning. In *ECCV*, pages 339–355. Springer, 2022. 2
- [41] Zhuosheng Zhang, Aston Zhang, Mu Li, and Alex Smola. Automatic chain of thought prompting in large language models. *arXiv preprint arXiv:2210.03493*, 2022. 2
- [42] Kaiyang Zhou, Jingkang Yang, Chen Change Loy, and Ziwei Liu. Conditional prompt learning for vision-language models. In *CVPR*, pages 16816–16825, 2022. 3
- [43] Kaiyang Zhou, Jingkang Yang, Chen Change Loy, and Ziwei Liu. Learning to prompt for vision-language models. *IJCV*, 130(9):2337–2348, 2022. 6
- [44] Deyao Zhu, Jun Chen, Xiaoqian Shen, Xiang Li, and Mohamed Elhoseiny. Minigt-4: Enhancing vision-language understanding with advanced large language models. *arXiv preprint arXiv:2304.10592*, 2023. 3

# Compositional Zero-shot Learning via Progressive Language-based Observations

## Supplementary Material

### Appendix

This supplementary document is organized as follows:

- The training and inference procedures of PLO-VLM and PLO-LLM are detailed in Sec. A.
- The observation generation prompts mentioned in Sec. 3.3 are illustrated in Sec. B.
- Implementation details referenced in Sec. 4.1 are provided in Sec. C.
- Additional quantitative results are presented in Sec. D.
- Additional qualitative results are displayed in Sec. E.
- Potential negative societal impacts are discussed in Sec. F.
- Limitations are considered in Sec. G.

### A. The procedures of Training and Inference

To provide a clearer understanding of our training and inference processes, we detail the specific operational steps of PLO-VLM and PLO-LLM in Algorithm 1 and Algorithm 2, respectively.

### B. Observation Prompt Generation

We present the prompt designed to generate a series of observation prompts that fed into the text encoder of CLIP within the framework of PLO-LLM. The prompt’s structure is as follows:

Setting: In compositional classification, we use the hostile prompt "a photo of [state] [object]" and compute similarities between images and prompts to determine composition category: [state] [object].

Q: How can you identify a photo of the composition "mashed banana" ? Please provide step-by-step observation prompts from easy to hard, where each step builds upon the previous one. Note that the last observation prompt is "a photo of mashed banana".

A: Let’s observe it step by step!

Four observation prompts:

- a photo of yellow, mushy substance
- a photo of a fruit that has been mashed into a paste
- a photo of a soft and creamy mixture made from bananas

---

### Algorithm 1: PLO-VLM Training and Inference

---

**Data:** Training data  $DS = \{(I, c)\}$   
**Result:** Optimal parameters for PLO-VLM

1 **Initialization:** Initialize weights;  
// Training Process

2 **while not converged do**

3     Sample a batch from  $DS$  with images  $\{I_k\}_{k=1}^n$   
   and their corresponding labels  $\{c_k\}_{k=1}^n$ ;

4     Extract  $\mathbf{v}$ ,  $\mathbf{t}_s$ ,  $\mathbf{t}_o$ , and  $\mathbf{t}_c$ ;

5     Use the pre-observing detector  $\mathcal{F}_{obs}^{pre}(\mathbf{v}, \mathbf{t}_s, \mathbf{t}_o)$   
   to determine observation order;

6     Compute  $\mathcal{L}_{obs}$ ;

7     **if observing object first then**

8         Obtain  $\mathbf{t}_{obs}^{pre} \leftarrow \mathbf{t}_o$ ,  $\mathbf{t}_{obs}^{post} \leftarrow \mathbf{t}_s$  ;

9         Compute refined  $\tilde{\mathbf{v}}$  via CA, based on  $\mathbf{t}_{obs}^{pre}$ ;

10         Compute  $p(s|I) = \pi(\mathcal{S}(\tilde{\mathbf{v}}, \mathbf{t}_{obs}^{post})$  ;

11         Compute loss for state:  $\mathcal{L}_s$ ;

12     **else**

13         Obtain  $\mathbf{t}_{obs}^{pre} \leftarrow \mathbf{t}_s$ ,  $\mathbf{t}_{obs}^{post} \leftarrow \mathbf{t}_o$  ;

14         Compute refined  $\tilde{\mathbf{v}}$  via CA, based on  $\mathbf{t}_{obs}^{pre}$ ;

15         Compute  $p(o|I) = \pi(\mathcal{S}(\tilde{\mathbf{v}}, \mathbf{t}_{obs}^{post})$  ;

16         Compute loss for object:  $\mathcal{L}_o$ ;

17     Compute  $p(c|I) = \pi(\mathcal{S}(\tilde{\mathbf{v}}, \mathbf{t}_c)$  and  $\mathcal{L}_c$ ;

18     Calculate total loss:  
    $\mathcal{L}_{PLO}^{VLM} = \mathcal{L}_{obs} + \mathcal{L}_s + \mathcal{L}_o + \mathcal{L}_c$ ;

19     Update weights using  $\mathcal{L}_{PLO}^{VLM}$ ;

// Inference Process

20 **for each test image I do**

21     Compute  $p(c|I)$ ;

22     Predict label:  $\hat{y}_c = \operatorname{argmax} p(c|I)$ ;

---

- a photo of mashed banana

Q: How can you identify a photo of the composition "{STATE CLASS} {OBJECT CLASS}" ? Please provide step-by-step observation prompts from easy to hard, where each step builds upon the previous one. Note that the last observation prompt is "a photo of {STATE CLASS} {OBJECT CLASS}".

A: Let’s observe it step by step!

Four observation prompts:

The prompt is divided into four individual parts: setting, constraint, example, and question:

- **Setting:** The setting text (*i.e.*, “In compositional

---

**Algorithm 2: PLO-LLM Training and Inference**

---

**Data:** Training data  $DS = \{(I, c)\}$   
**Result:** Optimal parameters for PLO-LLM

- 1 **Initialization:** Initialize weights;
- 2 **Observation Prompts Generation:**
- 3 **for** each composition category  $c \in C$  **do**
- 4     Generate observation prompts  $\mathcal{P}_c$  using LLM;
- // Training Process
- 5 **while** not converged **do**
- 6     Sample a batch from  $DS$  with images  $\{I_k\}_{k=1}^n$   
      and their corresponding labels  $\{c_k\}_{k=1}^n$ ;
- 7     **for** each observation step  $i$  **do**
- 8         Extract  $\mathbf{v}^{(i)}$  and  $\mathbf{t}_{obs}^{(i)}$ ;
- 9         Compute refined  $\tilde{\mathbf{v}}^{(i)}$  via CA and update  
           $\mathbf{v}^{(i+1)}$ ;
- 10        Compute probability:  
           $p(c^{(i)}|I, c^{(1)}, \dots, c^{(i-1)})$ ;
- 11     Calculate total loss:  $\mathcal{L}_{PLO}^{LLM} = \mathcal{L}_{step} + \mathcal{L}_c$ ;
- 12     Update weights using  $\mathcal{L}_{PLO}^{LLM}$ ;
- // Inference Process
- 13 **for** each test image  $I$  **do**
- 14     Compute  $p^{Soft}(c|I)$ ;
- 15     **for** each observation step  $i$  **do**
- 16         Update  $p^{Hard}(c|I)$  using hard prompts;
- 17     Predict label:  $\hat{y}_c = \operatorname{argmax} p(c|I)$ ;

---

classification...”) establishes a specific context and roles for the Large Language Models (LLMs) to operate within.

- **Constraint:** The constraint (*i.e.*, “Note that...”) outlines some limitations or constraints on the output generated by the LLMs.
- **Example:** The provided instance (*i.e.*, the example of “mashed banana”) functions as a guiding paradigm for the model to generate analogous output in the manner of in-context learning [4, 21].
- **Question:** The question (*i.e.*, “How can you identify...”) instructs the model to devise observation prompts tailored to the specific composition category under consideration.

In addition, this process adheres to the Chain-of-Thought concept [16, 41], generating observations step by step from easy to hard through the utilization of a special prompt “Let’s observe it step by step!”.

## C. Implementation Details

Our PLO models were trained and evaluated on one NVIDIA A100 GPU using PyTorch [32]. The GPT-3.5-turbo, a variant of the GPT model, known for its impressive

performance, was employed as the LLM. For the CLIP, we utilized OpenAI’s resources, opting for the Vision Transformer with a base configuration of ViT-L/14. In PLO-VLM, we assigned the weight factors for  $\mathcal{L}_{obs}$ ,  $\mathcal{L}_s$ ,  $\mathcal{L}_o$ , and  $\mathcal{L}_c$  to 1.0, 0.01, 0.01, and 1.0, respectively, as also presented in [22]. In PLO-LLM, the default number of observation prompts was set to 4. Further, fusion weights during the aggregation of probabilities for  $p^{Soft}(c|I)$  and  $p^{Hard}(c|I)$  were set to 0.7 and 0.3, respectively. Moreover, the weight factors assigned to  $\mathcal{L}_{step}$  and  $\mathcal{L}_c$  were both set to 1.0. Following [22], we used the Adam optimizer for 20 epochs on all datasets, with a learning rate of 2.5e-4 and a batch size of 64. In the open-world evaluation, we adhered to the post-training calibration method [30] to filter out compositions deemed infeasible. Our code will be released.

## D. Extra Quantitative Results

### D.1. Ablation Study on PEFT

**Setting.** To optimize the performance of PLO-VLM for CZSL tasks, we focused on enhancing CLIP’s image encoder using two distinct Parameter Efficient Fine-Tuning (PEFT) strategies: Adapter [6] and LoRA [7], the results are shown in Table 6. Below, we detail their integration into the image encoder of the CLIP.

**1) Adapter:** Adapters are particularly effective for our purpose as they introduce minimal parameters to the model, allowing us to fine-tune CLIP’s image encoder specifically for the CZSL tasks while avoiding overfitting. The Adapter layers are inserted between the transformer blocks of the image encoder, and they work as follows:

$$\text{Ada}(\mathbf{h}) = \mathbf{h} + \mathbf{U}(\text{ReLU}(\mathbf{D}(\mathbf{h}))), \quad (16)$$

where  $\mathbf{D}(\cdot)$  and  $\mathbf{U}(\cdot)$  are the downsampling and upsampling projection functions applied to the hidden states  $\mathbf{h}$ , with ReLU activation promoting non-linearity. The Adapter layers are optimized during training to adapt the pre-trained representations for better handling of the compositionality in CZSL.

**2) LoRA:** LoRA is applied to the self-attention modules within the CLIP’s image encoder to achieve a fine-tuning of attention mechanisms tailored to novel CZSL tasks. For each attention module, we modify its weight matrix  $\mathbf{W}$  using low-rank updates as follows:

$$\text{LoRA}(\mathbf{h}) = \mathbf{h} \times (\mathbf{W} + \delta\mathbf{W}), \quad (17)$$

where  $\delta\mathbf{W} = \mathbf{A}\mathbf{B}^T$  is the low-rank update with learnable matrices  $\mathbf{A}$  and  $\mathbf{B}$ . These updates are applied during fine-tuning, enabling the encoder to modify its attention patterns without altering the entire pre-trained weight structure.

These PEFT strategies are incorporated into the image encoder  $E_{n_v}(\cdot)$  by inserting learnable layers into its transformer blocks. This approach allows for fine-tuning on



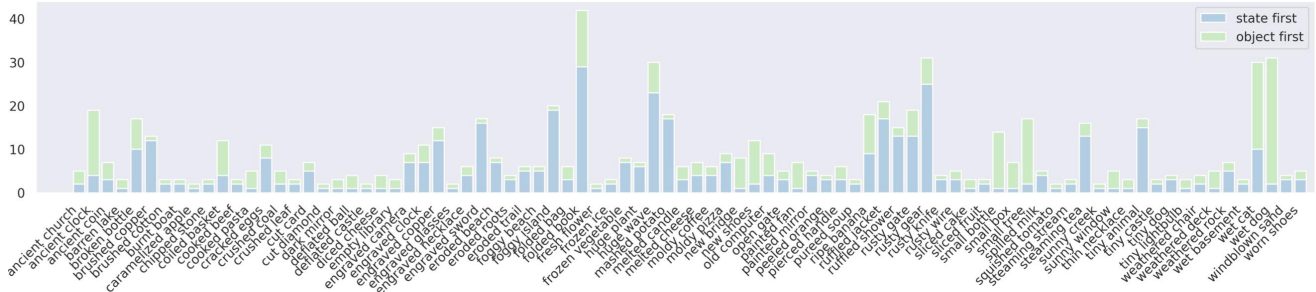


Figure 7. Distribution of samples where state or object is first observed in PLO-VLM on the test set of MIT-States.

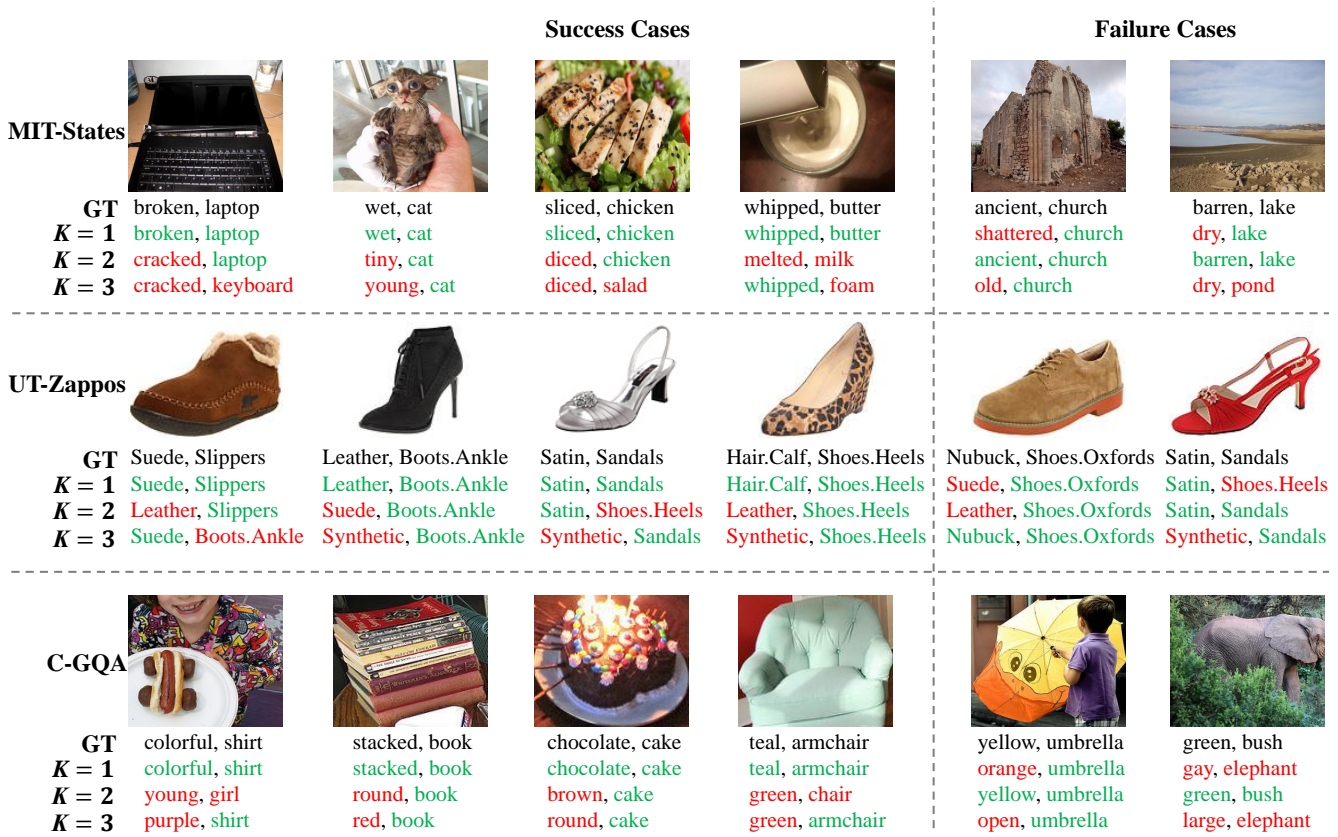


Figure 8. Top- $K$  predictions on for randomly selected cases from three datasets. The top and bottom rows show the results of closed-world settings, respectively. Correct and incorrect predictions are highlighted in green and red, respectively.

Strategy	MIT-States				UT-Zappos				C-GQA			
	S	U	HM	AUC	S	U	HM	AUC	S	U	HM	AUC
Adapter [6]	49.6	52.7	39.0	22.2	67.8	75.6	53.1	42.0	43.9	38.2	32.2	14.5
LoRA [7]	50.2	52.9	38.6	22.3	69.1	73.8	55.6	43.2	42.8	38.3	31.8	14.2

Table 6. Ablation study on different PEFT strategies in closed-world settings.

CZSL tasks while leveraging the rich feature extraction capabilities of CLIP’s pre-trained model.

**Results.** From Table 6, we can observe that both Adapter

and LoRA enhance CLIP for CZSL, with varying degrees of efficacy across different datasets. In the MIT-States dataset, LoRA outperforms Adapter in terms of seen, unseen, and

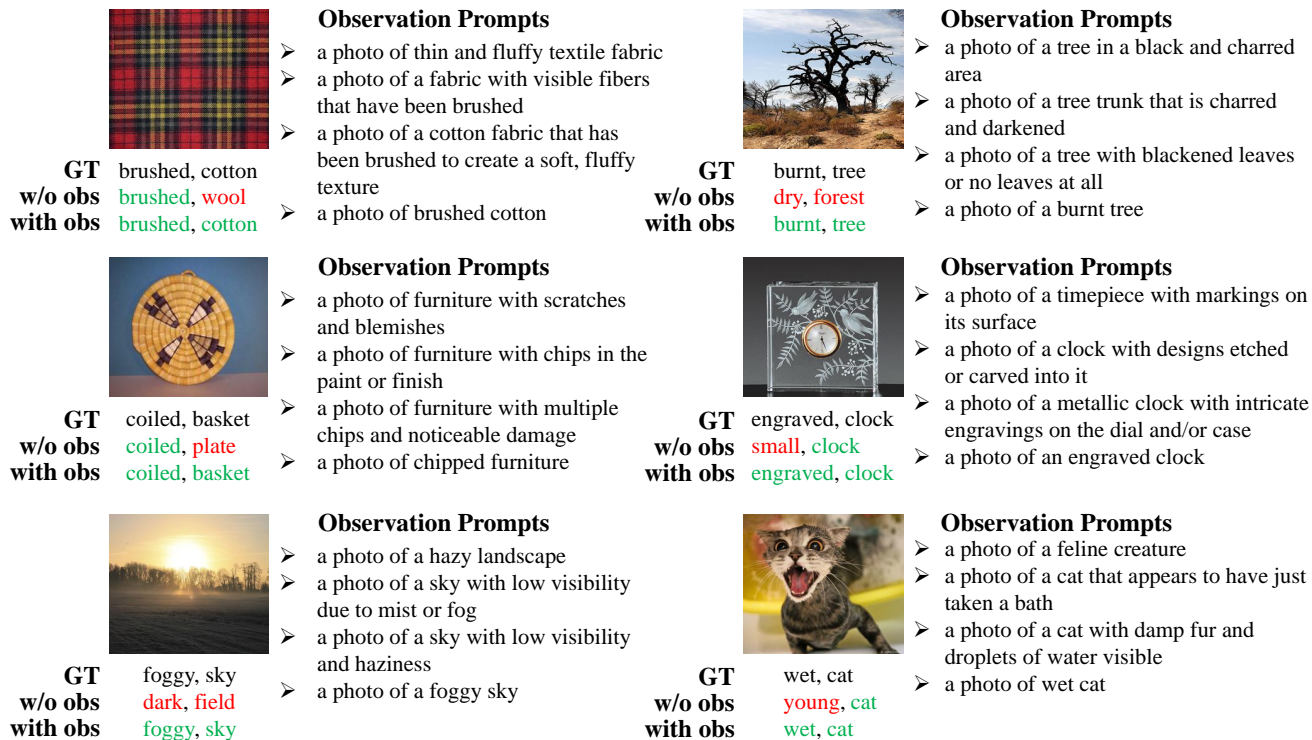


Figure 9. Top-1 predictions of PLO-LLM with and without multi-step observations under the closed-world setting on the MIT-States dataset. The corresponding generated observation prompts are presented to the right of each image. Correct and incorrect predictions are highlighted in green and red, respectively.

AUC metrics, while Adapter demonstrates slightly better performance in HM metric. On the UT-Zappos dataset, LoRA significantly exceeds Adapter, notably in seen and HM metrics. For the C-GQA dataset, the performance of both strategies is closely matched, with Adapter slightly leading in the seen and HM metrics.

## D.2. Observation Order in PLO-LLM

The bar chart in Figure 7 offers an extensive visualization of the frequency distribution for states and objects observed first within various composition categories on the MIT-States dataset. By presenting such a comprehensive statistic, we aim to provide an insightful reference that can aid future research endeavors in compositional learning and related fields.

## E. Extra Qualitative Results

**Success and Failure Cases.** Figure 8 displays the top- $K$  predictions from our PLO-VLM on the MIT-States, UT-Zappos, and C-GQA datasets. Successful cases, highlighted in green, demonstrate precise model predictions, exemplified by instances such as “sliced chicken”. Notably, some failures, marked in red, such as “gray elephant”, do not align with the ground truth (GT), yet still repre-

sent existing compositions within the image. These results underscore our model’s capability to identify state-object compositions, affirming its effectiveness in interpreting complex visual scenes despite occasional misalignments with the GT.

**Visualization results of PLO-LLM.** In Figure 9, we presented visualizations of the top-1 predictions obtained by PLO-LLM, in cases where observations (obs) were utilized or not. All results were from the MIT-States dataset under the closed-world setting. Concurrently, we displayed the sequence of step-by-step observation prompts on the right side of each image. With our meticulously designed prompt, the LLM effectively generated a progression of observation prompts that transitioned from easy to hard. Through the aid of these well-organized observation prompts, we empowered the model with *observing* capabilities, leading to better holistic understanding and considerable performance gains.

## F. Potential Negative Societal Impacts.

While the PLO-VLM and PLO-LLM models represent advancements in visual and linguistic AI applications, they may also have unintended societal impacts. The dependence of PLO on language models and vision-language pre-

training raises concerns about perpetuating incorrect or biased interpretations of compositions. This could occur if the underlying data or language prompts that inform these models are biased or flawed, leading to misrepresentations and potentially reinforcing stereotypes or inaccuracies.

## G. Limitations

Despite the promising results demonstrated by PLO-VLM and PLO-LLM in compositional zero-shot learning, we acknowledge two principal limitations: **1) Scope of Zero-Shot Learning:** Our approach primarily addresses the recognition of novel compositions involving already seen states and objects. It does not extend to the zero-shot recognition of entirely novel state and object categories. This limitation marks a boundary in our model’s applicability, underscoring the need for future developments that can generalize to entirely unseen states and objects. **2) Dependence on External Language Model APIs:** The efficacy of PLO-LLM is partly reliant on external language model APIs, such as those from OpenAI. This reliance introduces practical constraints, especially concerning the costs associated with API usage, which can escalate with the increase in the number of unique composition categories.